2002 #10

Development of Reaction Mechanism and Measurement of Burning Speed of Methane/Oxidizer/Diluent Mixtures at Low Temperatures and High Pressures

Faranak Rahim, Hameed Metghalchi
Mechanical, Industrial and Manufacturing Engineering Department
Northeastern University
Boston, Massachusetts

and

James C. Keck
Massachusetts Institute of Technology
Cambridge, Massachusetts

Proceedings of Western State Section of Combustion Institute Meeting,
San Diego, California, March 2002

Development of Reaction Mechanism and Measurement of Burning Speeds of Methane/Oxidizer/Diluent Mixtures at Low Temperatures and High Pressures

Faranak Rahim, Hameed Metghalchi
Mechanical, Industrial and Manufacturing Engineering Department
Northeastern University
Boston, Massachusetts
E-mail: metghal@coe.neu.edu

James C. Keck
Massachusetts Institute of Technology
Cambridge, Massachusetts

Abstract

Burning speeds of methane/air/diluent mixtures have been measured in a constant spherical volume chamber. A mixture of 86 % N_2 and 14 % CO_2 was used for the diluent to simulate the specific heat and molar mass of the exhaust gas. A thermodynamic model based on the conservation of mass and energy was used to calculate burning speed from the pressure rise due to the combustion process. The measurements covered the range of pressures from 1-25 atmosphere, unburned gas temperatures from 298-650 K, fuel/air equivalence ratios of 0.8 and 1.0 and diluent from 0-15%. The measured values have been compared to the theoretical values calculated by the PREMIX code developed by SANDIA. A reaction mechanism involving 53 species and 325 elementary reactions was taken from GRI-Mech 3.0. This mechanism is optimized for burned gas temperatures from approximately 1000 to 2500 K, pressures from 10 Torr to 10 atm., and equivalence ratio from 0.1 to 5. The comparison clearly demonstrated that the PREMIX / GRI-Mech 3.0 model predicts higher values in the high pressure/low temperature regime. Measurements in this domain differ quantitatively from the predictions of the model. The most probable reason for this is the omission of reactions involving alkyl peroxides in the GRI-Mech 3.0 kinetics.

Introduction

The laminar burning speed is a fundamental property of homogenous hydrocarbon/oxygen/diluent gas mixtures. It is of basic importance both for developing and testing chemical kinetic models of hydrocarbon oxidation and for a wide range of practical applications in the fields of engines, burners, explosions, and chemical processors.

A number of different methods have been used to experimentally determine the laminar burning speed. They can be characterized as being either constant pressure [1, 2] or constant volume [3, 4] methods. The constant pressure experiments, such as those made using flat flame burners [5] are limited to a relatively narrow range of temperatures and are most useful for obtaining data at atmospheric pressure. The disadvantages of the constant pressure experiments are that they provide data at only a single condition in each experiment and they also require significant corrections for conductive heat loss to the burner. The constant volume methods, such as combustion in a spherical chamber [3, 4], cover a much wider range of temperatures and pressures, provide a range of data along an isentrope in a single experimental run, and require very little correction for heat loss or other effects. Many researchers have used the spherical combustion chamber method for the determination of laminar burning velocities for a relatively wide range of fuels, diluent concentrations, pressures and temperatures. The flame dynamics, such as instabilities and stretch, which have been studied by many researchers [6-8], have subtle effects [7] and require more studies. Although at very high pressures these effects become more significant [9].

Measurements have been done for methane-air-diluent (In this study a mixture of 86 % N_2 and 14 % CO_2 is used) over the pressure range of 1-20 atm and temperature range of 298-650 K for equivalence ratios of 0.8-1.2. In the approach taken here, the pressure is the primary measurement. A thermodynamic analysis of the pressure time record that was used to calculate laminar burning speeds is presented in this paper. The measured values were compared to PREMIX [10] code's theoretical predictions using GRI-Mech 3.0 mechanism [11]. As it was expected, the agreement is very good at high

temperature, low pressure condition. GRI-Mech 3.0 predicts higher values at high pressure, low temperature conditions.

Experimental Setup and Methodology

The burning speed measurements have been made in the existing spherical and cylindrical combustion chambers [4, 12]. The spherical chamber consists of two hemispheric heads made from SAE 4140 alloy steel bolted together to make a 6.0-inch (15.4 cm) inner diameter sphere. The chamber is designed to withstand pressures up to 425 atm. and is fitted with ports for spark electrodes, diagnostic probes, and for filling and evacuating it. A thermocouple inserted through one of the chamber ports is used to check the initial temperature of the gas inside the chamber. A Kistler 603B1 piezo-electric pressure transducer with a Kistler 5010B charge amplifier is used to obtain dynamic pressure vs. time records from which the laminar burning speed is determined. Ionization probes mounted flush with the wall at the top and bottom of the chambers are used to measure the arrival time of the flame at the wall and check for spherical symmetry and buoyant rise.

The companion cylindrical chamber has a diameter and length equal to 5.25 inches which make its volume equal to that of the spherical chamber. The body is made of 304 stainless steel and the end windows are 1.0 inch thick boronsilicate. This chamber is designed to operate over the same pressure and temperature range as the spherical chamber and is equipped with similar access ports. The primary purpose of this facility is to permit optical observation of the flame shape and structure under conditions as close as possible to those in the spherical chamber and the initial development of the flame and pressure rise are identical in both chambers. A high speed CCD digital video camera, with variable speed of up to 8000 frames/second, is used for flame visualization. The gas handling system and acquisition system have been explained in previous papers [4, 12].

The theoretical model used to calculate the burning speed from the pressure rise in both chambers is based on one previously developed by Metghalchi and Keck [4, 12] with some modifications. In this model, gases in the chamber are divided into three parts [12]. The first is the burned gas in the center of chamber, the second is the unburned gas

around the burned gas, and the third is the wall boundary layer. Assumptions in this model have been explained in previous papers [4, 12]. Expansion of the burnt gas behind the flame front indicates a radial flow velocity S_g in the unburned gas causing the flame velocity S_f to be faster than the burning speed S_u by relation:

$$S_u = S_f - S_g \tag{1}$$

Figure 1 is showing the gas particle and flame front trajectories calculated for the stoichiometric methane-air mixture initially at atmospheric pressure and room temperature. The calculations were performed using the approximation of frozen combustion, constant specific heat and constant burning speed, hence, the results are not accurate but qualitatively demonstrate several aspects of the combustion process. First it can be seen that gas particles originally near the center of the bomb have been accelerated to a high velocity by the time they are overtaken by the flame front. After the particles is burned it has been pushed back towards the center, because of the compression and it will asymptotically go to its original location.

The laminar burning speed is defined by the equation

$$S_u = m\, \mathrm{v}_u \dot{x} / A_f \tag{2}$$

where:

S_u = Laminar burning speed

m = Mass of the gas mixture in the chamber

v_u = Specific volume of the unburned gas

$\dot{x}$ = Mass fraction burning rate

A_f = Flame area

The temperature and mass fraction of burned gas are determined using the equations for volume and energy [12]:

$$\frac{V}{m} = \int_0^x \mathrm{v}_b dx'' + \int_x^{x'} \mathrm{v}_{u_s} dx'' + \int_{x'}^1 \mathrm{v}_{b.l.} dx'' \tag{3}$$

$$\frac{E}{m} - \frac{Q}{m} = \int_0^x e_b dx'' + \int_x^{x'} e_{u_s} dx'' + \int_{x'}^1 e_{b.l.} dx'' \tag{4}$$

Where:

e : Specific internal energy.

E : Total initial energy of gas in the chamber.

Q : Energy transfer via heat interaction from boundary layer to the vessel.

x : Mass fraction burned.

x' : Total mass fraction of gases outside the boundary layer

x'' : Integration variable.

v : Specific volume.

V : Combustion chamber volume.

The subscripts b and u refer to the burned and unburned gas respectively and subscript $b.l.$ and s refer to boundary layer and isentropic process.

The mass of the gas mixture is determined from the measured initial composition, temperature, and pressure. Properties of the unburned gas such as specific internal energy and specific volume are determined using the JANAF Tables [13] and pressure measurements. The properties of the burned gases are determined using the JANAF Tables and the STANJAN [14] equilibrium code.

Flame curvature and stretch rate should also be considered in flame speed calculations. The curvature and stretch corrections are greatest when the flame radius is small and the flame thickness is of a similar order to the flame radius and it diminishes as the flame grows and gets thinner. Flame front thickness can be calculated by using the Rallis and Garforth [15] derivation:

$$\delta_f = \frac{4.6\overline{\lambda}}{\rho_u \overline{c}_p S_u} \qquad (5)$$

Where δ_f is the thickness of the preheat zone, $\overline{\lambda}$ is the average thermal conductivity of the mixture between unburned gas temperature and adiabatic flame temperature, $\overline{c}_p$ is the average specific heat at constant pressure and ρ_u is the unburned gas density. To calculate the average thermal conductivity, $\overline{\lambda}$, the thermal conductivity of each species is required. Thermal conductivity of each species is calculated using the Lennard-Jones parameters α and ε/k for methane, air etc. and the Hirschelfelder et al. [16] expression. These parameters have been obtained form the transport properties input

file of GRI-mech 3.0. Normalized flame thickness with respect to flame radius, for lean methane-air-diluent mixture has been calculated and shown in Figure 2. This mixture was initially at five atmosphere pressure, 5% diluent and equivalence ratio of 0.8. It can be observed that for normalized radii larger than 0.5 the ratio of flame thickness to flame radius is negligible (on the order of 10^{-4}) and consequently the stretch corrections are small. All measurements have been done for radii larger than ~50% radius of vessel. As the pressure increases the flame thickness decreases and this ratio will be even smaller at large radii.

Results and Discussion

The predictions of the GRI-Mech 3.0 model have been compared with flame speed measurements made in the spherical chamber for a wide range of conditions spanning both the high and low temperature regimes. The data used were limited to cases where corrections for stretch and curvature were negligible, i.e. flame radius much greater than flame thickness. The conditions under which significant "cracking" or wrinkling occurred, were observed and are reported.

Figure 3 shows a comparison between measured and calculated values of the burning speeds for stoichiometric methane-air mixtures at 1 atm pressure vs. unburned gas temperature. The experimental results for constant volume chambers were been obtained using the power law fit [4] to the data. It can be seen that for these conditions which are in the high temperature regime, the PREMIX calculations are in excellent agreement with experimental results from this study. Previously measured values reported by Kurata et al. [17], Iijima et al. [18] and Sharma et al. [19] and Gottgens et al. [20] are also shown.

Figure 4 shows the burning speeds along isentropes for stoichiometric methane-air-diluent mixtures with initial pressures of 1 atm and diluent of 0-15%. Again the agreement is good with PREMIX calculations. Also in this figure the values of power law fit to the experimental data have been shown along with the actual data.

Figure 5 shows the effect of diluent on the measured and calculated burning speeds along isentropes for methane-air-diluent at an equivalence ratio of $\phi = 0.8$, initial

temperature of 300 K and initial pressure of 5 atmosphere. Adding diluent reduces the burned gas temperature making the flame slower and moving it deep into the low temperature/high pressure regime. As it can be seen, the agreement between calculations and experimental results is poor. In the case of 0 and 5% diluent the measured values are crossing the PREMIX predictions. As the amount of diluent is increased to 10 and 15%, PREMIX predicts higher values.

Flame propagation of a stoichiometric methane-air-diluent mixture in the cylindrical vessel (P_i = 1 atm, T_i = 300 K) is shown in Figure 6 part a. Inside the vessel, pressure reaches approximately 8 times its initial value before the flame hits the wall. It can be seen that throughout the whole experiment, the flame is smooth and spherical for this particular mixture. At high pressures, the flame front is cellular and instabilities can be observed even at smaller radii, shown in Figure 6 part b. In this figure, the methane-air mixture is at higher pressure (P_i = 5 atm). It is shown in this figure that at pressure ratio (P/P_i) of 1.26, cells start to grow on the flame surface. This might be the reason for the higher measured values than PREMIX calculations in Figure 5. In Figure 6 part c and d, flame propagation of methane-air-diluent mixtures (P_i of 5 atm, T_i of 300 K) with 5 and 15% diluent respectively, have been shown. Instabilities can be observed around pressure ratio of 1.6 in part c. For methane-air mixture with 15% diluent, the flame is stable due to excess nitrogen. With higher nitrogen diluent smooth flames with only a few large wrinkles were observed. Measurements have been done only up to the point that flame hits the top wall. Ionization probes mounted flush with the wall at the top and bottom of the chambers are used to measure the arrival time of the flame at the wall and check for spherical symmetry and buoyant rise.

The GRI-Mech 3.0 reaction mechanism differs from measured values in low-temperature/high-pressure regime. A possible reason for this is the failure to include reactions of the type

$$\dot{C}H_3 + O_2 + (M) \xleftrightarrow{A} CH_3\dot{O}_2 + (M)$$

$$CH_3\dot{O}_2 + H\dot{O}_2 \longleftrightarrow CH_3O_2H + O_2$$

$$CH_3O_2H \longleftrightarrow CH_3\dot{O} + \dot{O}H$$

which will be important at high pressure, low temperature condition. The competing reaction to reaction "A" at high temperature, low pressure is:

$$\dot{C}H_3 + O_2 \xleftarrow{B} CH_3\dot{O} + \dot{O}$$

which is included in GRI-Mech 3.0 model. The reaction "A" which is dependent of pressure is essentially a chain termination and is competing with reaction "B". At some pressure and temperature, the rate of reaction "A" will exceed the rate of reaction "B" and that is where the GRI mechanism fails. However, a temperature increase shifts the reaction "A" and $CH_3\dot{O}_2$ decomposes.

Reaction rates R_A and R_B are defined as

$$R_A = k_A[CH_3][O_2][M]$$
$$R_B = k_B[CH_3][O_2]$$

where k_A is a function of pressure and k_B is a temperature dependent rate coefficient.

Using any of the existing methods to get the reaction coefficient of A and using the Arrhenius parameters for reaction B, the temperature-pressure that $R_A / R_B = 1$ can be found. This locus has been shown in Figure 7. In order to draw the locus number one, the Lindemann [21] approximation was used to calculate k_A. In the second curve Keck's approximation and in the third curve, Westbrook's parameter [22] was used. The disagreement between these different methods is due to approximating the reaction rate constant and it proves the uncertainties in the reaction kinetics. This figure illustrates the temperature-pressure region of burned gases for different mixtures can be located either above or under this line or it can cross it. Above the $R_A / R_B = 1$ line the GRI mechanism will be the controlling mechanism but below the line a modified GRI mechanism should be considered. It can be seen that for mixtures with higher diluent the dominant mechanism will be some modified mechanism that include the alkyl-peroxide reactions with correct reaction kinetics.

Concluding Remarks

We have successfully demonstrated the need of a modified mechanism for high pressure low temperature conditions. The above results clearly demonstrated that the

PREMIX/GRI-Mech 3.0 model predicts higher values of burning speed in the high pressure/low temperature regime. Measurements in this domain differ from the predictions of the model. The most probable reason for this is the omission of reactions involving alkyl peroxides in the GRI-Mech 3.0 kinetics. Other investigators have also seen disagreement between measured burning speeds and calculations using GRI-Mech 3.0 model at high pressures [9]. As it is mentioned in Rozenchan et al. further work is needed to identify the causes of these deviations.

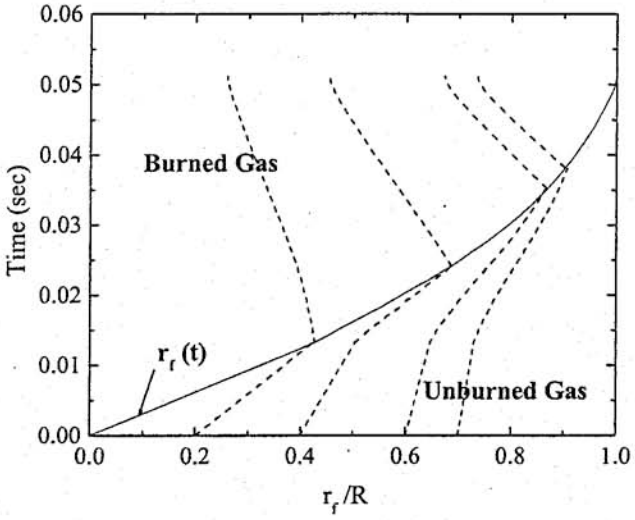

Figure 1- Gas particles and flame front trajectories, methane-air, ϕ = 1.0, initilal pressure of 1 atm and initial temperature of 300 K.

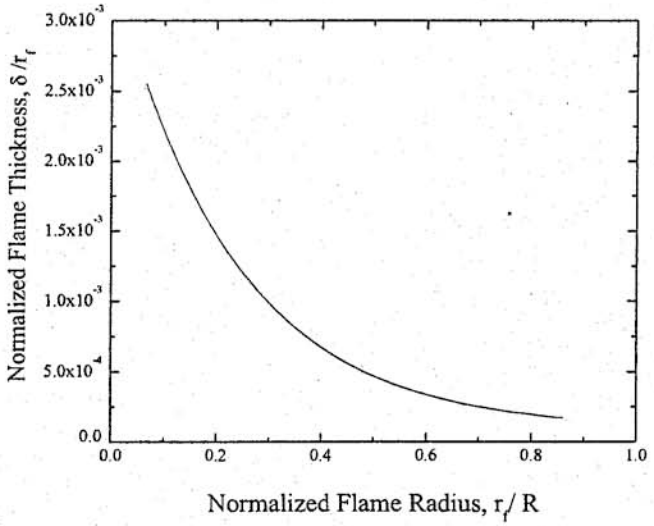

Figure 2- Normalized flame thickness vs. normalized flame radius of methane-air-diluent mixture with 5% diluent, initial pressure of 5 atm and initial temperature of 300 K.

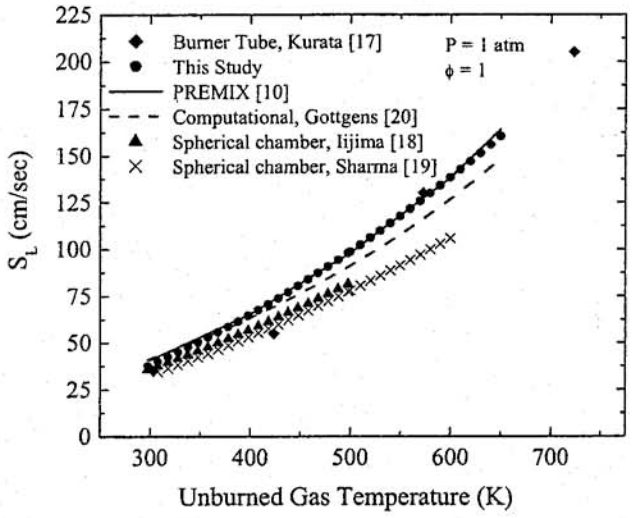

Figure 3- Comparison of burning speed of methane-air mixtures with those determined by Kurata et al. [17], computational PREMIX code [10], Gottgens et al. [20], Iijima et al. [18] and Sharma et al. [19] at 1 atm.

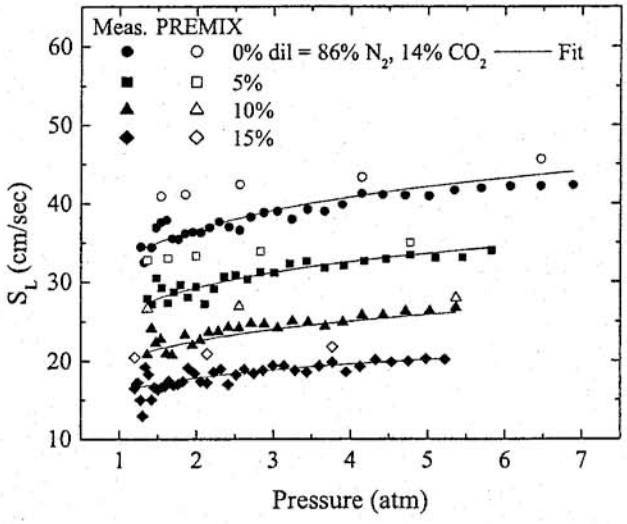

Figure 4- Comparison of burning speed of stoichiometric methane-air-diluent mixtures with those determined by PREMIX code [10] along isentropes with initial pressure of 1 atm and initial temperature of 300 K, with different diluent percentage.

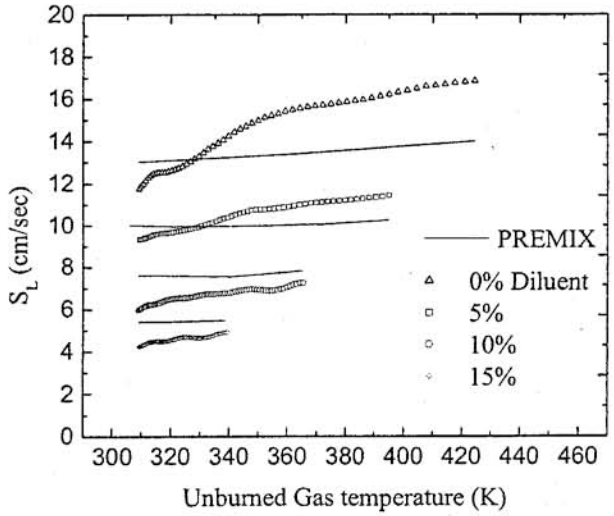

Figure 5- Comparison of burning speed of methane-air-diluent mixtures with those determined by PREMIX code [10] along isentropes with initial pressure of 5 atm and initial temperature of 300 K, with different diluent percentage.

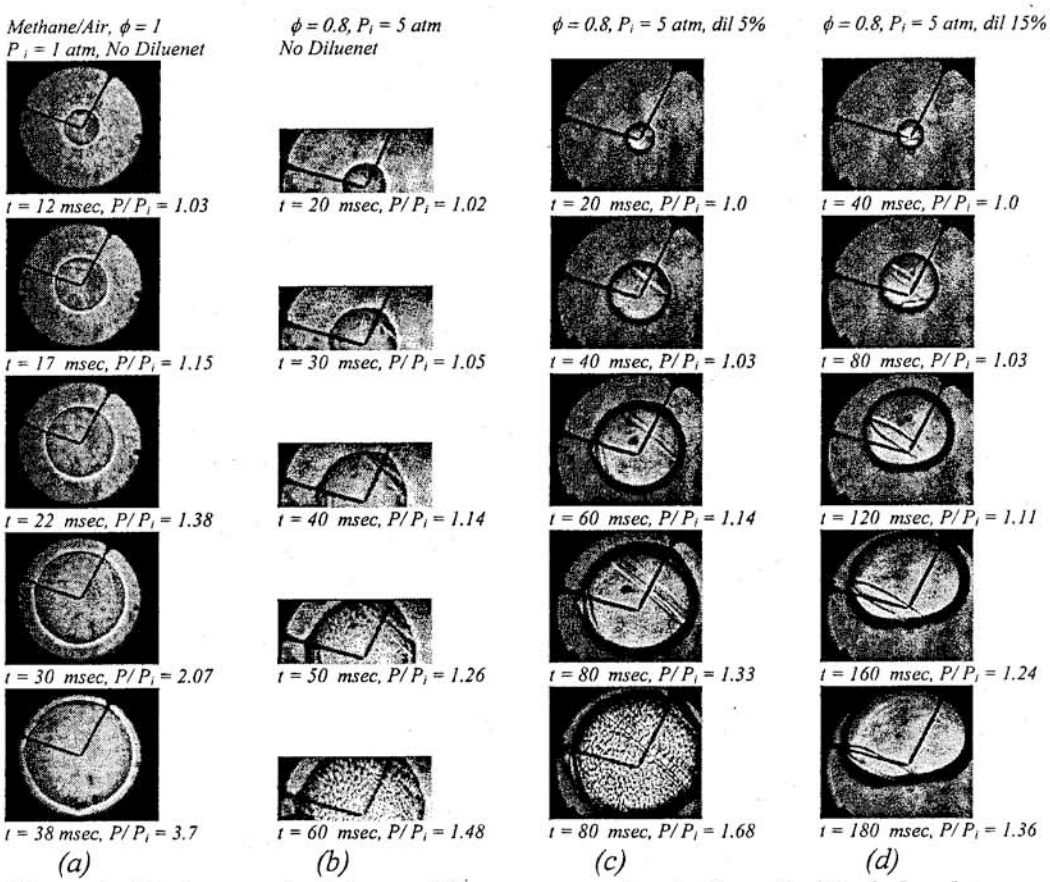

Figure 6- Shadowgraph pictures of flame propagation in the cylindrical chamber .

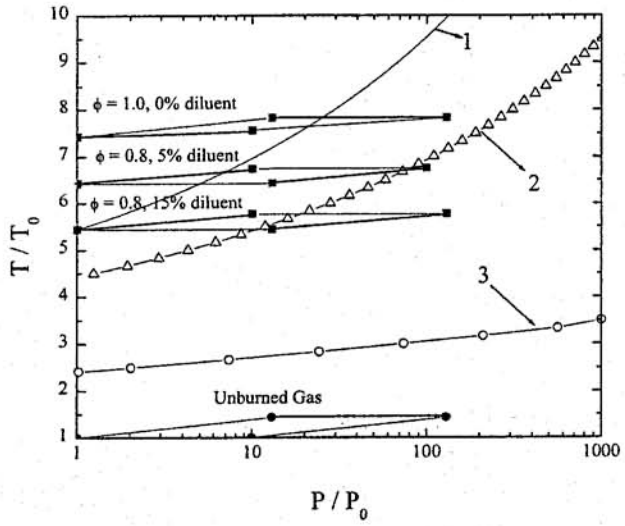

Figure 7- Locus of R_A/R_B = 1. Locus 1, 2 and 3 have been calculated using Lindemann approximation, Keck's approximation and Westbrook's reaction rate constants respectively.

References

1. Kwon, S., Tseng, L., and Faeth, G. Laminar burning velocities and transmission to unstable flames in H_2 / O_2 / N_2 and C_3H_8 / O_2 / N_2 mixtures, *Combustion and Flame,* 1992, 90, 230-246.
2. Tseng, L., Ismail, M., and Faeth, G. Laminar burning velocities and Markstein numbers of hydrocarbon / air flames, *Combustion and Flame,* 1993, 95, 410-426.
3. Shebeko, Y., Tsarichenko, A., Trunev, A., Navzenya, V., Papkov, S., and Zaitzev, A. Burning velocities and flammability limits of gaseous mixtures at elevated temperatures and pressures, *Combustion and Flame,* 1995, 102, 427-437.
4. Elia, M., Ulinski M., Metghalchi, M. Laminar burning velocity of methane-air-diluent mixtures, *ASME Journal of Engineering for Gas Turbines and Power,* 2001, 123, 190-196.
5. Van Maaren, A., Thung, D. and Goey, L. Measurement of flame temperature and adiabatic burning velocity of methane/air mixtures, *Combustion Science and Technology,* 1994, 96, 327-344.
6. Gu X. J., Haq M. Z., Lawes M. and Woolley R. Laminar burning velocity and Markstein lengths of methane-air mixtures, *Combustion and Flame,* 2000, 121, 41-58.
7. Hassan M. I., Aung K. T. and Faeth G. M. Measured and predicted properties of laminar premixed methane/air flames at various pressures, *Combustion and Flame,* 1998, 115, 539-550.
8. Bradley, D., Gaskell P. H., and Gu, X. J. Burning velocities, Markstein lengths, and flame quenching for spherical methane-air flames: a computational study, *Combustion and Flame,* 1996, 104, 176-198.
9. Rozenchan, D., Tse, S. D., Zhu, D. L., Law, C. K. Laminar burning rates and Markstein lengths of CH_4/O_2/inert mixtures at high pressures, *39th Aerospace Sciences Meeting and Exhibit, AIAA,* Jan 8-11, 2001, Reno, NV.
10. Kee, R. J., Grcar, J. F., Smooke, M. D. and Miller, J. A., Sandia Report SAND85-8240, 1985.

11. Smith, G. P., Golden, D. M., Frenklach, M., Moriarty, N. W., Eiteneer, B., Goldenberg, M., Bowman, C. T., Hanson, R. K., Song, S., Gardiner Jr., W. C., Lissianski, V. V. and Qin, Z., http://www.me.berkeley.edu/gri_mech/
12. Rahim, F., Elia, M., Ulinski, M., Metghalchi, M., Burning velocity measurements of methane-oxygen-argon mixtures and its application to extend methane-air burning velocity measurements, *International Journal of Engine Research*, In Press, 2002.
13. JANAF Thermochemical Tables, Third Edition. American Chemical Institute, American Institute of Physics, National Bureau of Standards 1986.
14. Reynolds, W. C., Stanford University Report, ME 270, no 7, 1986.
15. Rallis C. J., Garforth A. M. The determination of laminar burning velocity, *Progress in Energy and Combustion Science,* 1980, 6, 303-329.
16. Hirschfelder, J. O., Curtiss, C. F., and Bird, R. B., Molecular Theory of Gases and Liquids, John Wiley & Sons, Inc., New York, 1967.
17. Kurata, O., Takahashi, S., and Uchiyama, Y. Influence of preheat temperature on the laminar burning velocity of methane-air mixtures, *Journal of SAE*, 1994, 119-125.
18. Iijima, T., and Takeno, T. Effects of temperature and pressure on burning velocity, *Combustion And Flame,* 1986, 65, 35-43.
19. Sharma, S. P., Agrawal, D. D., and Gupta, C. P. The pressures and temperature dependence of burning velocity in a spherical combustion bomb, *Eighteen Symposium (International) on Combustion*, 1981, 493-501.
20. Gottgens, J., Mauss, F., Peters, N. Analytic approximation of burning velocities and flame thickness of lean hydrogen, methane, ethylene, ethane, acetylene, and propane flames, Twenty-Fourth Symposium (International) on combustion Institute, 1992, 129-135.
21. Lindemann, F. A., *Trans. Faraday Soc.*, 17, 598 (1922).
22. Westbrook, C.K.,http://www-cms.llnl.gov/combustion/combustion2.html.